Molecular Basis of Cell and Developmental Biology:

Replicative Senescence Induced by Romo1-derived Reactive Oxygen Species

Young Min Chung, Seung Baek Lee, Hyung Jung Kim, Seon Ho Park, Jung Jin Kim, Jin Sil Chung and Young Do Yoo

J. Biol. Chem. 2008, 283:33763-33771.
doi: 10.1074/jbc.M805334200 originally published online October 3, 2008

THE JOURNAL OF BIOLOGICAL CHEMISTRY VOL. 283, NO. 48, pp. 33763–33771, November 28, 2008

Replicative Senescence Induced by Romo1-derived Reactive Oxygen Species*

Received for publication, July 14, 2008, and in revised form, September 26, 2008 Published, JBC Papers in Press, October 3, 2008, DOI 10.1074/jbc.M805334200

Young Min Chung[‡1], Seung Baek Lee[‡1], Hyung Jung Kim[§], Seon Ho Park[‡], Jung Jin Kim[‡], Jin Sil Chung[‡], and Young Do Yoo[‡2]

From the [‡]Graduate School of Medicine and Brain Korea 21 Program for Biomedical Science, Korea University College of Medicine, Korea University, Seoul 136-705 and the [§]Department of Internal Medicine, Yonsei University College of Medicine, Seoul 135-270, Republic of Korea

Persistent accumulation of DNA damage induced by reactive oxygen species (ROS) is proposed to be a major contributor toward the aging process. Furthermore, an increase in age-associated ROS is strongly correlated with aging in various species, including humans. Here we showed that the enforced expression of the ROS modulator 1 (Romo1) triggered premature senescence by ROS production, and this also contributed toward induction of DNA damage. Romo1-derived ROS was found to originate in the mitochondrial electron transport chain. Romo1 expression gradually increased in proportion to population doublings of IMR-90 human fibroblasts. An increase in ROS production in these cells with high population doubling was blocked by the *Romo1* knockdown using *Romo1* small interfering RNA. *Romo1* knockdown also inhibited the progression of replicative senescence. Based on these results, we suggest that age-related ROS levels increase, and this contributes to replicative senescence, which is directly associated with Romo1 expression.

The chromosomal ends of senescent cells are associated with DNA damage-response factors. Telomere shortening triggers a DNA damage checkpoint response, resulting in replicative senescence. Blocking of the DNA damage checkpoint response releases cell cycle arrest in the G_1 phase of the cell (1). One of the important mediators in telomere-dependent senescence is p53, and it plays an important role in DNA damage response as well as regulation of cellular senescence. The other main regulators of senescence are reported as $p21^{WAF1/CIP1}$, $p16^{INK4A}$, and retinoblastoma protein, and these have been classified into two major signaling pathways, the p53/$p21^{WAF1/CIP1}$ pathway and the $p16^{INK4A}$/retinoblastoma protein pathway (2).

ROS[3] are continuously produced in response to both endogenous and exogenous stimuli inside the cell (3). Even though poor regulation of ROS production could lead to various pathological disorders, low levels of ROS are indispensable for many biological processes such as mitogenic proliferation (4, 5). ROS have been known to be the main mediator and inducer of cellular senescence and organismal aging (6). Hydrogen peroxide treatment of cells triggers senescence-like growth arrest, and oxidative damage correlates with senescence of human fibroblast cells (7, 8). ROS induce cellular senescence not only by triggering DNA damage but also by activating redox-sensitive pathways (9). It was suggested that oxidative stress shortened the telomere length through DNA single strand breaks (10). Increased oxidants trigger oxidative DNA damage, and such oxidants are sensed by the DNA damage-response pathway, which is a common mediator of senescence (6). The oxidative DNA damage in promoters of genes that are down-regulated with age has been known to be associated with human brain aging (11).

ROS are generated from the electron transport chain in the mitochondria, which is the main source of ROS (3). Many studies have reported that ROS derived from the mitochondria are directly involved in replicative senescence. Intracellular ROS levels were increased with age, and this is associated with mitochondrial dysfunction (12). The down-regulation of genes related to mitochondrial function was also observed in the aging human brain (11). Mitochondrial dysfunction was detected in hepatocytes from old rats, in which low mitochondrial membrane potential and increased ROS levels were observed (13). In accordance with these results, Zahn *et al.* (14) observed that genes involved in the mitochondrial electron transport chain pathway are down-regulated with age in several species, including humans.

Mitochondrial dysfunction is correlated with an accumulation of mtDNA mutations, which contributes to aging and degenerative diseases (15). Mutations and deletions of mtDNA were observed during aging (16, 17). Increased mutations and

* This work was supported by Grant FG06-2-20 from the 21st Century Frontier Functional Human Genome Project funded by the Korea Government (MEST), by Grant R01-2006-000-10113-0 from the Basic Research Program of the Korea Science and Engineering Foundation, and by Grant R11-2005-017-01001-0 from the Research Center for Woman's Diseases of the Korea Science and Engineering Foundation. The costs of publication of this article were defrayed in part by the payment of page charges. This article must therefore be hereby marked "*advertisement*" in accordance with 18 U.S.C. Section 1734 solely to indicate this fact.

[1] Both authors contributed equally to this work.

[2] To whom correspondence should be addressed: Korea University College of Medicine, Anam Hospital, 126-1, 5ka, Anam-dong, Sungbuk-ku, Seoul 136-705, Korea. Tel.: 82-2-920-5762; Fax: 82-2-920-5762; E-mail: ydy1130@korea.ac.kr.

[3] The abbreviations used are: ROS, reactive oxygen species; Romo1, reactive oxygen species modulator 1; siRNA, small interfering RNA; PDL, population doublings; DCF-DA, 2′,7′-dichlorofluorescein diacetate; NAC, *N*-acetylcysteine; H_2O_2, hydrogen peroxide; JC-1, 5,5′,6,6′-tetrachloro-1,1′,3,3′-tetraethylbenzimidazolcarbocyanine iodide; SA-β-gal, senescence-associated β-gal; MFP, mifepristone; ΔΨm, mitochondrial membrane potential; DSBs, double-strand breaks; PBS, phosphate-buffered saline; TRITC, tetramethylrhodamine isothiocyanate; Gy, gray; RT, reverse transcription.

deletions of mtDNA in mice with defective mitochondrial DNA polymerase are associated with reduced life span (18). There have been many reports that gene mutations in the mitochondrial electron transport chain produce high levels of oxidants and are correlated with aging. Increased superoxide production was observed in the skin fibroblast containing complex I (NADH-CoQ reductase) deficiency (19). A mutation in the succinate dehydrogenase cytochrome *b* large subunit in complex II was reported to produce superoxide (20). The increased ROS production resulting from this mtDNA mutation demonstrated a role in life span (21). A mutation of the succinate dehydrogenase cytochrome *b* subunit causes premature aging in nematodes (21). Furthermore, the inactivation of the *COX5* gene of the respiratory complex IV decreases ROS production and prolongs life span (22). A mutation in the iron-sulfur protein (*isp*-1) also decreases sensitivity to ROS and increases the life span (23). One other study also showed that the targeted mutation of $p66^{Shc}$ extended the murine life span (24). $p66^{Shc}$, which is located in the mitochondria, produces mitochondrial ROS in response to proapoptotic signals (25).

In accordance with the above studies, transgenic mice overexpressing catalase in the mitochondria extend murine life span (26). These results demonstrated that oxidative stress in the mitochondria is associated with aging. However, no correlation reports between mitochondrial ROS production and longevity were also reported in *Drosophila* and $Sod2^{+/-}$ mice (27, 28). In a previous study, we identified a novel protein termed Romo1, which was shown to localize to the mitochondria. We also showed that enforced Romo1 expression enhanced ROS production (29). Through further investigation, we reported that Romo1 was responsible for up-regulated ROS levels in cancer cells and that Romo1-derived ROS was required for cancer cell proliferation as well as normal cells such as IMR-90 human fibroblasts (5). Because increased ROS levels and oxidative damage are both implicated as the major contributors toward senescence, this study was undertaken to investigate the expression of *Romo1* in senescent cells and whether Romo1-derived ROS played a role in cellular senescence.

EXPERIMENTAL PROCEDURES

Cell Culture and Reagents—The human lung fibroblast IMR-90 cell line was obtained from the American Type Culture Collection (ATCC, Manassas, VA), and cells were maintained in Eagle's minimal essential media. Human lung cancer cells (H1299) were cultured in RPMI 1640 medium (Invitrogen). All media contained 10% heat-inactivated fetal bovine serum (Invitrogen), sodium bicarbonate (2 mg/ml; Sigma), penicillin (100 units/ml), and streptomycin (100 μg/ml; Invitrogen). 2′,7′-Dichlorofluorescein diacetate (DCF-DA), *N*-acetylcysteine (NAC), H_2O_2, stigmatellin, myxothiazol, and rotenone were purchased from Sigma. MitoSOX, dihydrorhodamine 123, MitoTracker Red, and 5,5′,6,6′-tetrachloro-1,1′,3,3′-tetraethylbenzimidazolylcarbocyanine iodide (JC-1) were obtained from Molecular Probes (Eugene, OR).

Senescence-associated (SA) β-Galactosidase Assay—Cellular senescence was examined using a senescent cell staining kit (Sigma). SA-β-galactosidase staining was performed according to the manufacturer's instructions.

Small Interfering RNA Assay—Romo1 siRNA designed to target *Romo1* (30) was synthesized by Bioneer (Taejon, Republic of Korea) and was transfected into IMR-90 cells using Lipofectamine 2000 (Invitrogen).

RNA Preparation and Northern Blotting—Total RNA was extracted from each sample using TRIzol reagent (Invitrogen). After 10 μg of the total RNA was resolved on a 1% agarose/formaldehyde gel, the RNA samples were transferred into a Nytran N nylon membrane (Schleicher & Schuell). The *Romo1* cDNA probe (29) was labeled with a random primer DNA labeling kit (Roche Applied Science). Hybridization was performed overnight at 68 °C.

Measurement of Intracellular ROS by Flow Cytometry—The fluorescence intensity of the DCF-DA-stained cells was measured by a FACScan flow cytometer (BD Biosciences). The cells were cultured for 2 days in the presence of control siRNA or Romo1 siRNA and then incubated with 50 μM DCF-DA at 37 °C for 30 min, and intracellular fluorescence of 5,000 cells was measured by flow cytometry using the green fluorescence emission parameter. ROS levels were also measured using dihydrorhodamine 123 (5 μM) and MitoSOX (5 μM).

Measurement of Mitochondrial Membrane Potential—To determine changes of mitochondrial membrane potential after Romo1 induction, H1299/pGene-Romo1 cells (29) treated with mifepristone (MFP) were incubated with JC-1 (5 μM) for 30 min at 37 °C. JC-1 was excited at 490 nm, and emission fluorescence was filtered, and images were collected at fluorescein isothiocyanate (green, 530 nm) and TRITC channels (red, 590 nm) using the LSM510 (Zeiss). The images were analyzed using LSM 3.5 image analysis software (Zeiss).

Western Blot Analysis—Western blotting was performed using anti-p53 (DAKO, Denmark), anti-$p21^{WAF1/CIP1}$ (Santa Cruz Biotechnology), anti-$p16^{INK4a}$ (Santa Cruz Biotechnology), and anti-β-actin (Sigma) antibodies as described previously (31). Blots were visualized using chemiluminescence (ECL kit, Amersham Biosciences).

ROS Assays—For ROS measurement using SpectraMax (Molecular Devices, Sunnyvale, CA), 2×10^4 cells were plated onto 12-well plates. DCF-DA was added to cell culture media and incubated at 37 °C for 30 min. After the cells were rinsed with phosphate-buffered saline (PBS; pH 7.4), intracellular ROS levels were measured at a 490 nm excitation wavelength and at a 535 nm emission wavelength using SpectraMax. ROS fluorescence intensity was normalized by the cell number, which was counted using trypan blue staining.

Fluorescence Microscopy—MitoSOX (5 μM) was added to cell culture media, and excess probes were removed by rinsing with PBS. Coverslips were wet-mounted onto slides, and fluorescent images from multiple fields of view were captured using a fluorescence microscope (Olympus LX71 microscope).

Confocal Microscopy—After treatment, the cells grown on the chambered cover glass were washed twice with PBS and incubated with MitoTracker Red (50 nM). DCF-DA was added directly to the cell cultures and incubated at 37 °C for 30 min to detect ROS. The fluorescence images from multiple fields of view were obtained using an Axioplan II microscope (Zeiss) and a confocal microscope (MRC-1024 MP, Bio-Rad, and LSM510, Zeiss), which were set at the designated exposure setting. For

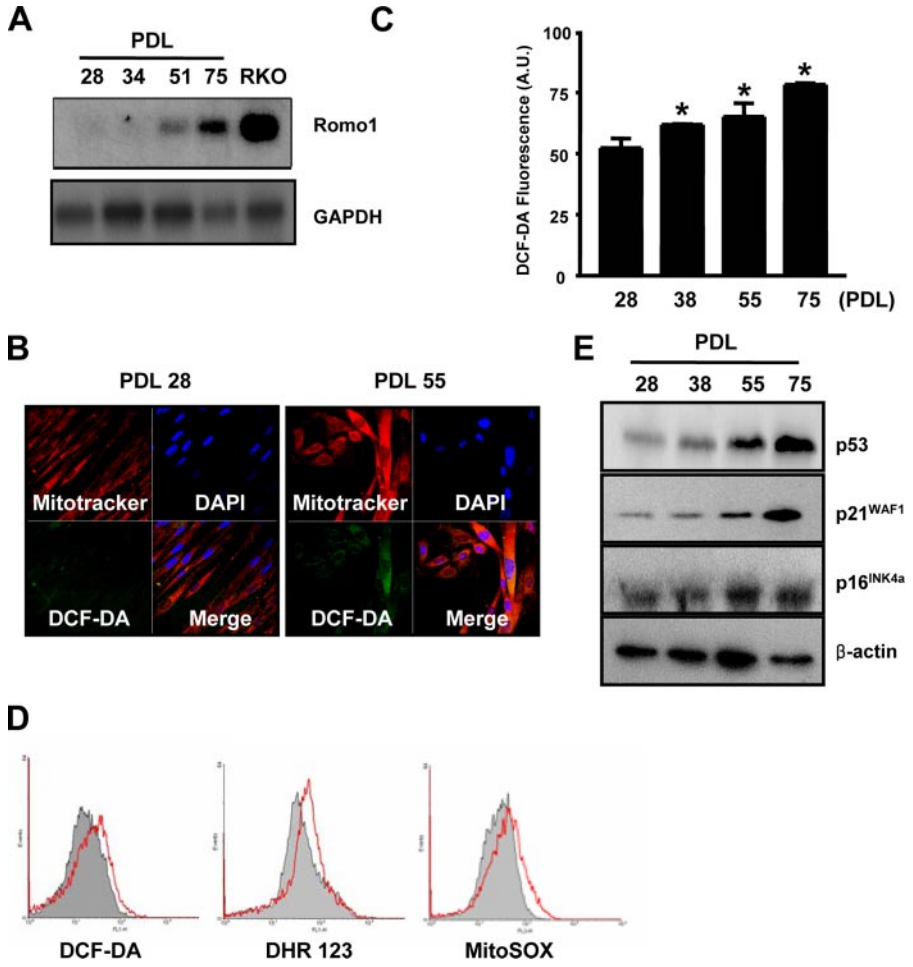

FIGURE 1. **Increased *Romo1* and ROS levels in IMR-90 cells with high PDL.** *A, Romo1* expression in IMR-90 cells with various PDL. To determine the *Romo1* expression level in IMR-90 cells, Northern blot analysis was performed by hybridization with a 245-bp ^{32}P-labeled BamHI-XhoI fragment of *Romo1* or human *GAPDH* probe. *B,* IMR-90 cells (PDL 28 and PDL 55) were stained with MitoTracker or DCF-DA, and ROS levels were determined by confocal microscopy. *DAPI*, 4′,6-diamidino-2-phenylindole. *C,* ROS levels in IMR-90 cells with various PDL were measured by SpectraMax using DCF-DA. Relative ROS levels were normalized by cell counting using trypan blue. Results represent mean (±S.E.) of three independent experiments performed in triplicate. *, $p < 0.05$ *versus* the IMR-90 (PDL 28) cells. *D,* ROS levels in cells were measured by fluorescence-activated cell sorter analysis after staining with the fluorescent probes. The *gray curves* indicate IMR-90 cells with PDL 32, and the *red curve* indicates IMR-90 cells with PDL 67. *E,* protein samples (30 μg/ml) were separated using 12% SDS-PAGE and transferred onto nitrocellulose membranes. Immunodetection was performed using anti-p53, anti-p21$^{WAF/CIP1}$, anti-p16^{INK4a}, and anti-β-actin antibodies. *A.U.* refers to artificial units.

foci analyses, the cells were first fixed, permeabilized, and blocked. The foci were observed by immunolocalization using the anti-phospho-H2AX (1:200, Upstate Biotechnology) antibody diluted in 1% bovine serum albumin/PBS/Triton X-100. The immune complexes were then stained with Alexa Fluor 594-conjugated goat anti-rabbit IgG (1:500, Molecular Probes). After 4′,6-diamidino-2-phenylindole staining and mounting, fluorescence images were obtained using Zeiss Axioplan II and confocal microscopy. The images were analyzed using LSM 3.5 image analysis software (Zeiss) and Confocal Assistant software (version 4.02, Bio-Rad).

Analysis of DNA Damage by Alkali Comet Assay—The cells were treated with either H_2O_2 (200 μM) or IR (10 Gy), and the H1299/pGene-Romo1 cells were induced by MFP. A Comet Assay kit (Trevigen) was used according to the manufacturer's instructions. For the comet assay, electrophoresis was performed at 1 V/cm and 30 mA for 60 min. The ratios of DNA in the head and tail of the comets were analyzed. Eighty randomly selected cells per sample were examined.

Transmission Electron Microscopy—The cells were cultured until they reached 50% confluency and were then treated with MFP for 24 h with or without NAC (0.5 mM). The cells were washed twice with PBS and centrifuged at 1,000 rpm for 5 min. The samples were fixed in 2% osmium tetroxide for 2 h, and stained *en bloc* with a uranyl acetate coloration solution for 90 min. After dehydration with increasing concentrations of ethanol and propylene oxide, thin sections were sliced using the Reichert ultracut and mounted on 200-mesh copper grids. These were then stained with 2% uranyl acetate and 1% lead citrate for 12 min each. The grids were observed under a Hitachi H-7500 electron microscope, and images were captured at a final magnification of ×15,000.

Statistical Analysis—Each assay was performed in triplicate and was independently repeated at least three times. Statistical analysis was conducted using the Student's analysis of variance. Statistical significance was defined as $p < 0.05$. Means, S.E., and p values were calculated using GraphPad PRISM, version 4.02 for Windows (GraphPad Software, San Diego).

RESULTS

Romo1 Expression Was Increased in Senescent Cells—Romo1 was reported to generate ROS in the mitochondria (29). Therefore, we were curious as to whether *Romo1* expression was increased during the progression of senescence of IMR-90 cells. Northern hybridization was conducted to examine *Romo1* expression in these cells. Interestingly, *Romo1* expression was enhanced in the cells at PDL 51, and higher *Romo1* expression was observed in the cells at PDL 75 (Fig. 1*A*). Increased ROS formation was observed in cultured endothelial cells with high PDL, and this was concurrent with other studies reporting elevated ROS levels with age (12, 32). We examined ROS levels in old IMR-90 cells. IMR-90 cells that had been continuously cultured were stained with DCF-DA, and the ROS levels were examined by confocal microscopy. Increased DCF-DA staining was observed in the cells at PDL 55 (Fig. 1*B*), which corresponded to increased ROS levels. The increased ROS formation was quantified using a microfluorometer plate reader, and the relative ROS increase is shown in Fig. 1*C*. ROS levels were also meas-

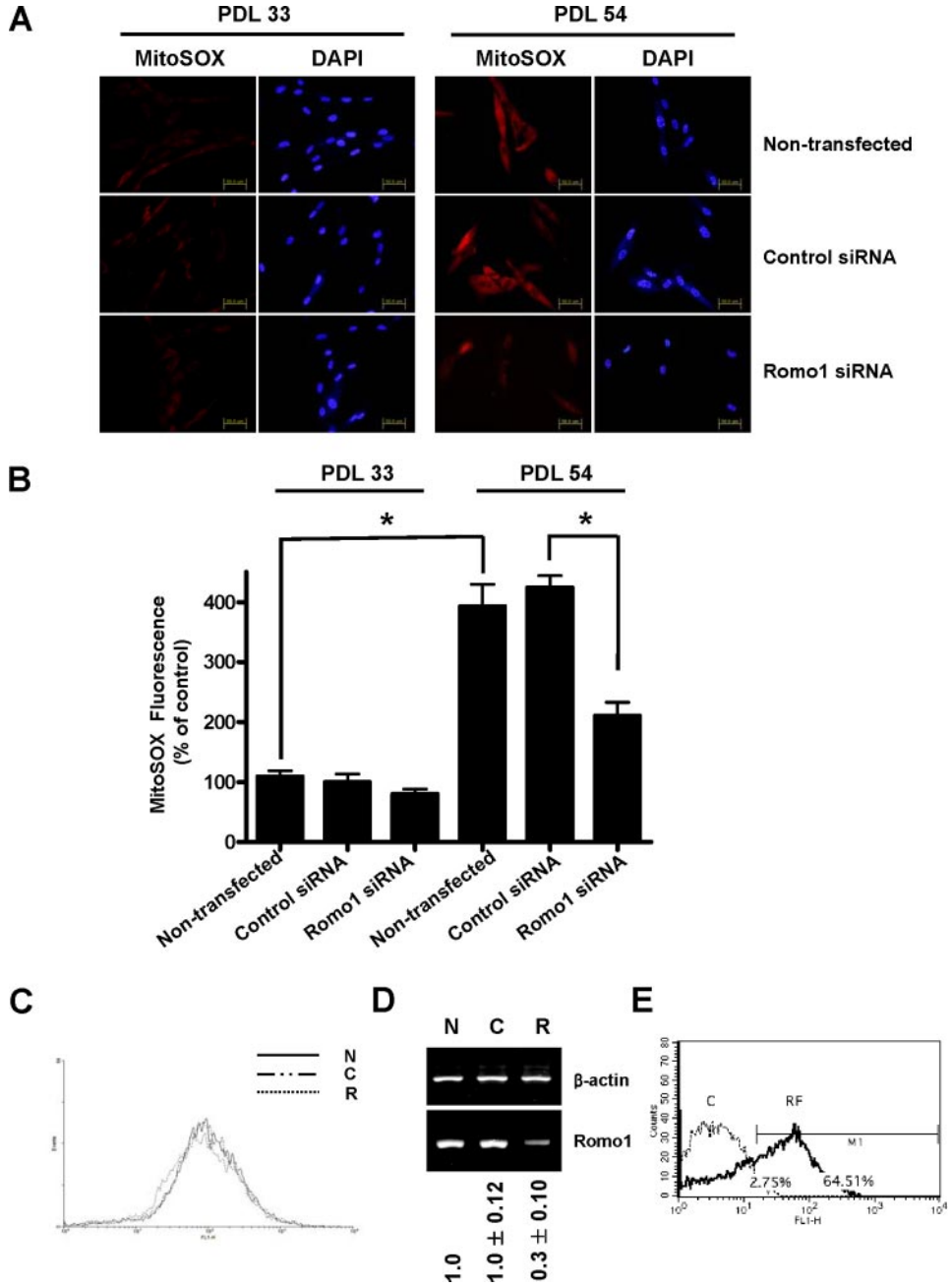

FIGURE 2. **ROS down-regulation by *Romo1* siRNA transfection.** *A,* fluorescence microscopy images of ROS down-regulation by *Romo1* siRNA (100 nM) transfection. IMR-90 cells (PDL 33 and PDL 54) were stained with MitoSOX (5 μM). *DAPI*, 4′,6-diamidino-2-phenylindole. *B,* measurement of mitochondrial ROS production. Data were acquired and analyzed using Metamorph software (Universal Imaging, Westchester, PA). *, $p < 0.01$. *C*, IMR-90 cells (PDL 52) were transfected with *Romo1* siRNA and stained with DCF-DA. ROS down-regulation was analyzed by flow cytometry. *D, Romo1* knockdown by *Romo1* siRNA transfection in IMR-90 cells. *Romo1* siRNA (100 nM) or control siRNA (100 nM) were transfected into IMR-90 cells, and the cells were harvested after 48 h. *Romo1* knockdown was examined by RT-PCR. β-Actin was used as a loading control. *E,* flow cytometric analysis. *Romo1* siRNA-fluorescein isothiocyanate was transfected into IMR-90 cells, and the transfection efficiency was analyzed by flow cytometry. *N,* nontransfected cells; *C,* cells transfected with control siRNA; *R,* cells transfected with *Romo1* siRNA; *RF,* cells transfected with *Romo1* siRNA-fluorescein isothiocyanate.

sion of these proteins was gradually up-regulated during continuous culture of IMR-90 cells.

Romo1 Expression Was Responsible for ROS Increase in Senescent Cells—We then tried to determine whether Romo1-induced ROS was responsible for ROS increase in cells with high PDL. As shown in Fig. 2*A*, enhanced ROS levels were observed in IMR-90 cells at PDL 54, and transfection with *Romo1* siRNA blocked this increase in ROS formation. The production of mitochondrial ROS in the IMR-90 cells was quantified using the Metamorph software (Fig. 2*B*). ROS reduction by *Romo1* siRNA was also observed by flow cytometry (Fig. 2*C*). These results demonstrated that Romo1 played a major role in the regulation of ROS in IMR-90 cells with high PDL. IMR-90 cells, which are human normal lung fibroblast cells, are quite difficult to transiently transfect with plasmids, and such experiments are usually conducted in the presence of a drug selection. To observe the transfection efficiency of IMR-90 cells, we examined *Romo1* knockdown by RT-PCR (Fig. 2*D*) and measured transfection efficiency by flow cytometry (Fig. 2*E*). *Romo1* knockdown was conducted by RT-PCR, but not by Northern blot techniques, because of the low expression of *Romo1* expression (29). Fig. 2*E* showed that *Romo1* siRNA was efficiently transfected into IMR-90 cells and that the transfection efficiency of *Romo1* siRNA was greater than 60%.

Increased Romo1 Expression Induced Senescence—To test whether Romo1 expression triggered cellular senescence of IMR-90 cells, retrovirus expressing Romo1 was infected into the cells and treated with G418. Ten days later, SA-β-galactosidase activity was measured. As shown in Fig. 3, *A* and *B*, Romo1 expression induced cellular senescence.

ured by flow cytometry, and the same results were obtained, as shown in Fig. 1*D*. The shift to the right of the curve because of increased fluorescence indicated an increase in the intracellular ROS levels. Because p53, $p21^{WAF/CIP1}$, and $p16^{INK4a}$ expression were enhanced in cells with high PDL (33, 34), this was examined by Western blot analysis. Fig. 1*E* showed that the expression of these proteins was gradually up-regulated during continuous culture of IMR-90 cells.

H-Ras was used as a positive control. Fig. 3*C* shows that Romo1 expression enhanced intracellular ROS level, and H-Ras also increased the cellular ROS level. Fig. 3*C, right column,* shows the merged images of ROS and mitochondria stained with MitoTracker. A hybrid gene encoding *Romo1* tagged with Myc (Romo1-myc) was used in this experiment,

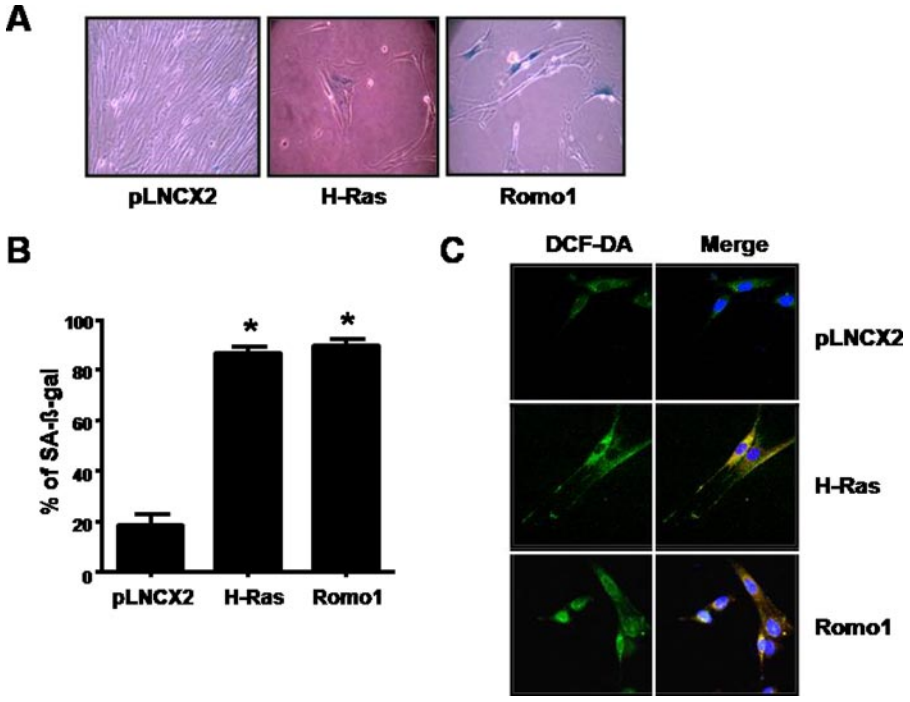

FIGURE 3. **Romo1-induced senescence of IMR-90 cells.** *A,* retrovirus expressing Romo1 or H-Ras was infected into IMR-90 cells and treated with G418 (200 μg/ml). Acidic β-galactosidase activity was measured after 10 days. *B,* senescent cells were counted under an inverted microscope. Results represent mean (±S.E.) of three independent experiments performed in triplicate. *, $p < 0.05$ *versus* pLNCX2. *C,* Romo1-induced ROS production. Cells were infected with retrovirus expressing H-Ras or Romo1 and stained with DCF-DA. The level of ROS production was examined by confocal microscopy. The *left column* indicates DCF-DA staining, and *right column* indicates the merged images of DCF-DA staining and MitoTracker staining.

and Romo1-myc protein expression was examined by Western blot analysis using the anti-Myc antibody (29). These results demonstrated that Romo1 expression was increased during progression of cellular senescence, and increased Romo1 expression induced cellular senescence.

Next, we examined whether the increase of Romo1-derived ROS formation was associated with replicative senescence of IMR-90 cells. The cells were transfected with 40 nM *Romo1* siRNA because 100 nM *Romo1* siRNA inhibited cell growth (5). As shown in Fig. 4, *Romo1* siRNA transfection delayed replicative senescence. As a positive control, the cells were treated with NAC. NAC treatment inhibited replicative senescence, and this result was consistent with previous reports (32).

Romo1 Induced Nuclear DNA Damages—Because oxidative DNA damage is sensed by the DNA damage-response pathway and is known to be a common mediator of senescence (6), we examined whether Romo1-triggered ROS induced DNA damage. Romo1-induced DNA damage was examined by observation of the formation of γ-H2AX foci. The production of γ-H2AX foci after irradiation was confirmed by irradiating the IMR-90 cells with 10 Gy and examining the foci using immunofluorescence microscopy after staining the cells with the anti-γ-H2AX antibody. As shown in Fig. 5*A*, irradiation induced the formation of foci in the nuclei of the IMR-90 cells. A similar observation was made in the IMR-90 cells treated with H_2O_2. The IMR-90 cells were then transfected with *Romo1* to determine whether Romo1 induced the formation of γ-H2AX foci. The introduction of *Romo1* induced the formation of γ-H2AX foci, which was abolished by NAC treatment, demonstrating that the ROS generated by Romo1 caused DNA damage (Fig. 5*B*). The Romo1-induced formation of γ-H2AX foci formation was confirmed by treating the stably transfected H1299/pGene-Romo1 cells containing an MFP-inducible expression system (29) with MFP and counting the number of foci. As shown in Fig. 5*C*, MFP treatment induced the formation of γ-H2AX foci. The γ-H2AX foci began to form after 12 h and reached a maximum of 48 h after the MFP treatment (Fig. 5*D*). The double strand breaks (DSBs) generated by the Romo1-induced ROS were also examined using a comet assay. As a positive control, the IMR-90 cells were irradiated, and the tail moment was analyzed (Fig. 6*A*). The tail moment formed by Romo1-induced ROS was also observed in the H1299/pGene-Romo1 cells treated with MFP (Fig. 6*B*). The tail moment was detected from 12 h and increased in a time-dependent manner (Fig. 6*C*).

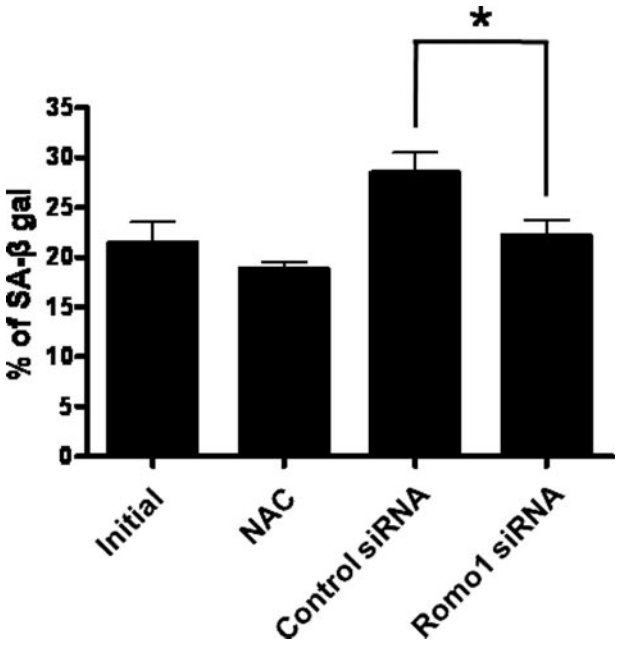

FIGURE 4. **Inhibition of senescence progression by *Romo1* knockdown.** After 1×10^5 cells (PDL 34) were seeded on a cover glass in a 6-well cell culture plate, cells were transfected with control siRNA (40 nM) and *Romo1* siRNA (40 nM) using Lipofectamine 2000. The cells were treated with 10 μM NAC for 2 h and repeated every 48 h. *Romo1* siRNA was transfected into the cells, and transfection was repeated again 4 days later. Ten days later, SA-β-galactosidase assay was performed to estimate the senescence level. Result represents mean (±S.E.) of the three independent experiments performed in triplicate. *, $p < 0.05$.

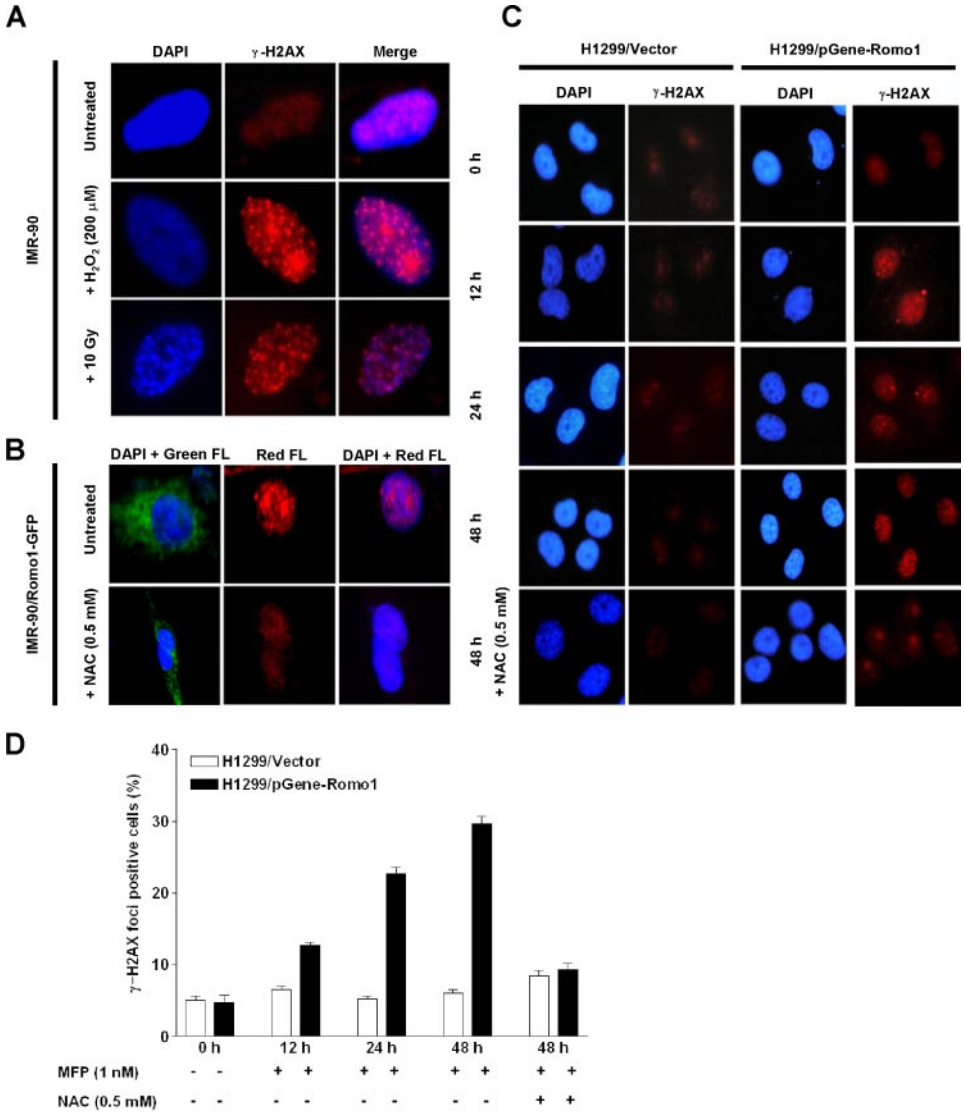

FIGURE 5. **Romo1 induced DNA damage in the IMR-90 and H1299 cells.** *A*, γ-H2AX foci formation (*red, middle columns*) in normal IMR-90 cells treated with either IR (10 Gy) or H_2O_2 (200 μM) were examined by confocal microscopy. *DAPI*, 4′,6-diamidino-2-phenylindole. *B*, IMR-90 cells were transiently transfected with *Romo1*-GFP, and the Romo1 expression level was examined by confocal microscopy (*left column, green*). The increased γ-H2AX foci formation (*red, middle columns*) was examined after *Romo1* transfection. In the *lower panels*, the decreased foci formation of γ-H2AX was examined in cells preincubated with NAC (0.5 mM). *C*, H1299/pGene-Romo1 cells were treated with MFP (1 nM), and the increased formations of γ-H2AX foci (*red fluorescence*) were examined. The decreased formation of γ-H2AX foci was examined in the cells preincubated with NAC (0.5 mM). *D*, time course analysis of DNA damage (γ-H2AX foci formation) in H1299/pGene-Romo1. The cells were treated with MFP (1 nM), and the γ-H2AX foci in the cells were examined at 12, 24, and 48 h. The foci in at least 200 cells were counted, and the data represent the mean (± S.E.) of three experiments performed in triplicate.

Romo1-derived ROS Originated from the Mitochondrial Respiratory Chain—Because Romo1 localizes to the mitochondria (29), we examined whether Romo1-enhanced ROS production originated from the mitochondrial respiratory chain. The superoxide generation by Romo1 induction was observed by MitoSOX, a mitochondrial superoxide indicator, staining. A Romo1-inducible cell line (H1299/pGene-Romo1) was used in this study. The cells were induced by MFP and treated with specific inhibitors of the respiratory complexes. The levels of ROS production were quantified by incubating the mitochondria with MitoSOX. As shown in Fig. 7, *A* and *B*, ROS levels were increased after Romo1 induction, and ROS production was blocked by stigmatellin or myxothiazol treatment, which inhibited ROS production at complex III. Rotenone, an inhibitor of the electron transport at complex I, and malonate, a complex II inhibitor, failed to inhibit ROS production, suggesting that the Romo1-induced production of ROS occurred within complex III of the electron transport chain. A previous study showed that morphological changes in the mitochondria, in the form of a round and swollen shape, were observed in some of the Romo1-GFP expressing H1299 cells (29). These changes were also observed by electron microscopy. As shown in Fig. 7*C*, the intermembrane spaces of many mitochondria appeared to be widened. This mitochondrial structural reorganization may be triggered by Romo1-induced ROS production because NAC treatment was shown to have blocked the Romo1-induced mitochondrial cristae remodeling. An increase in the levels of ROS in the mitochondria may cause the opening of the mitochondrial permeability transition pore, resulting in the collapse of the mitochondrial membrane potential (ΔΨm) (35). To test whether Romo1-triggered ROS production induced ΔΨm changes, the cells were treated with MFP and stained with the ΔΨm-sensitive dye JC-1. As a positive control, the cells were treated with H_2O_2. In H_2O_2-treated cells, the JC-1 dye remained in the cytoplasmic green fluorescence of the monomeric form, indicating a low ΔΨm (Fig. 7*D*). Fig. 7*D* also indicates the merged image of red fluorescence and green fluorescence, showing a yellow color. Increased Romo1 induction caused a ΔΨm, decrease and treatment with mitochondrial inhibitors blocked any changes in ΔΨm (Fig. 7*D*). These results demonstrated that enhanced ROS levels induced by increased Romo1 expression originated from complex III of the mitochondrial respiratory chain and that this may cause mitochondrial dysfunction.

DISCUSSION

Although ROS levels increased by various stresses could lead to various pathological disorders, an appropriate ROS level is indispensable for cell proliferation (4). The concentration of H_2O_2 is intracellularly maintained from a low of ~0.001 μM to a high of ~0.7 μM (36). Antioxidant treatment inhibited cell

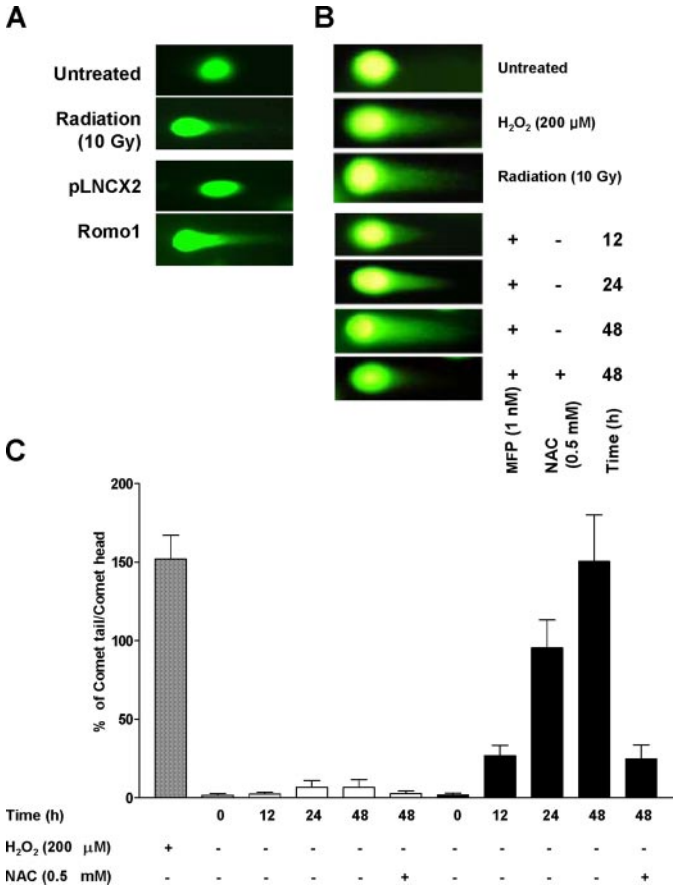

FIGURE 6. **Comet assay.** *A,* comet assay was performed in the IMR-90 cells infected with retrovirus expressing Romo1. As a positive control, the IMR-90 cells were irradiated with IR (10 Gy). *B,* comet assay was performed in the H1299/pGene-Romo1 cells treated with MFP (1 nM). The H1299/pGene-Romo1 cells were treated with MFP, and the time course analysis of the comet assay was analyzed. *C,* length of the comet tail per length of the comet head, which was defined as DNA damage, was measured in at least 80 cells per sample. The data represent the mean (±S.E.) of at least three independent experiments performed in triplicate.

growth by decreasing endogenous ROS levels (37). This cell growth inhibition was because of the arrest of the cell in the G_1 phase (38) resulting from the up-regulation of cyclin-dependent kinase inhibitors, such as $p21^{WAF/CIP1}$ and $p16^{INK4a}$, and down-regulation of G_1 cyclins (39). Although treatment of the cells with a high dose of H_2O_2 induced cell growth inhibition or death, treatment of cells with a low dose of H_2O_2 increased cell proliferation by activating the extracellular signal-regulated kinase (40–42). In a previous study, we also showed that down-regulation of ROS by *Romo1* knockdown induced cell cycle arrest at the G_1 phase and inhibition of cyclin D1 expression (5).

Romo1 was first identified in 2006, and Romo1 expression was shown to be up-regulated in most cancer cell lines (29). A recent publication (43) reported that a high level of ROS derived from the mitochondria was detected in cancer cells. Therefore, we were curious to test if the high levels of ROS observed in many cancer cells originated from Romo1 in our previous study and showed that *Romo1* knockdown decreased ROS levels not only in various cancer cells but also in IMR-90 cells (5). This study demonstrated that Romo1-derived ROS was needed for normal and cancer cell proliferation. However, the exact mechanism of ROS production remains to be elucidated. In subsequent experiments, we observed that *Romo1* expression was increased in the IMR-90 cells with high PDL and that its expression was up-regulated in proportion to increasing PDL (Fig. 1*A*). We wondered if Romo1-induced ROS contributed to replicative senescence of IMR-90 cells. Because ROS are the major inducers of replicative senescence, and antioxidant treatment was shown to delay the senescence of endothelial cells (32), we tested whether Romo1-induced ROS affected replicative senescence. Even though the expression of *Romo1* was undetectable in IMR-90 cells by Northern blot analysis (29), we were able to analyze the level of *Romo1* expression by RT-PCR (Fig. 2*C*). Romo1-derived ROS is indispensable for normal cell proliferation because *Romo1* siRNA transfection inhibited IMR-90 cell growth (5). It appeared that Romo1, which is expressed in low levels in normal cells, produced a small amount of ROS needed for cell proliferation. Therefore, we were unable to use a sufficient amount of *Romo1* siRNA for *Romo1* knockdown in this study. We also observed that transfection of 100 nM *Romo1* siRNA twice for 10 days inhibited growth of the IMR-90 cells (data not shown). In this study, low amounts of *Romo1* siRNA were transfected into IMR-90 cells, such that severe growth inhibition was not induced. Although replicative senescence of the cells transfected with 40 nM *Romo1* siRNA was partially delayed in Fig. 4, we suggest that ROS derived from increased Romo1 expression plays an important role in replicative senescence of IMR-90 cells.

It is known that ROS generated from the mitochondria are major determinants of cellular senescence and organismal aging (44). Mitochondrial function declines with aging. Low $\Delta\Psi m$ and increased ROS levels were observed in hepatocytes from old rats (12, 13). In this study, we showed that enforced Romo1 expression triggered cristae remodeling of mitochondria and induced $\Delta\Psi m$ down-regulation. Romo1 induced cristae remodeling of the mitochondria, and $\Delta\Psi m$ down-regulation was triggered by ROS generated from Romo1 because antioxidant treatment blocked Romo1-induced cristae remodeling of the mitochondria and $\Delta\Psi m$ down-regulation. From these results, we suggest that Romo1 expression is enhanced during aging and that ROS levels derived by Romo1 cause mitochondrial dysfunction, resulting in replicative senescence.

ROS levels, which cause single strand nicks and DSBs, are up-regulated with age and can cause an increase in 8-oxo-dG generation in various species (44). DSBs are often observed in senescent cells and aged mice. Sedelnikova *et al.* (45) showed that many DNA lesions with DSBs in senescent cells, which are irreparable, were observed in nontelomeric regions and suggested that persistent DNA lesions with irreparable DSBs are an important factor that causes aging. This study showed that ROS produced by increased Romo1 expression induced nuclear DNA damage. To accomplish this, ROS should be released into the cytosol. Even though the majority of ROS in the mitochondria are produced at complexes I and III, it has been reported that complex III is a major source of ROS released into the cytosol (46). Fig. 7 shows that stigmatellin and myxothiazol, which inhibits the electron transport at complex III, blocked Romo1-induced production of ROS. An analysis of a hypothetical translation using the "Translate" program on the EXPASY website indicated that Romo1 is a transmembrane protein.

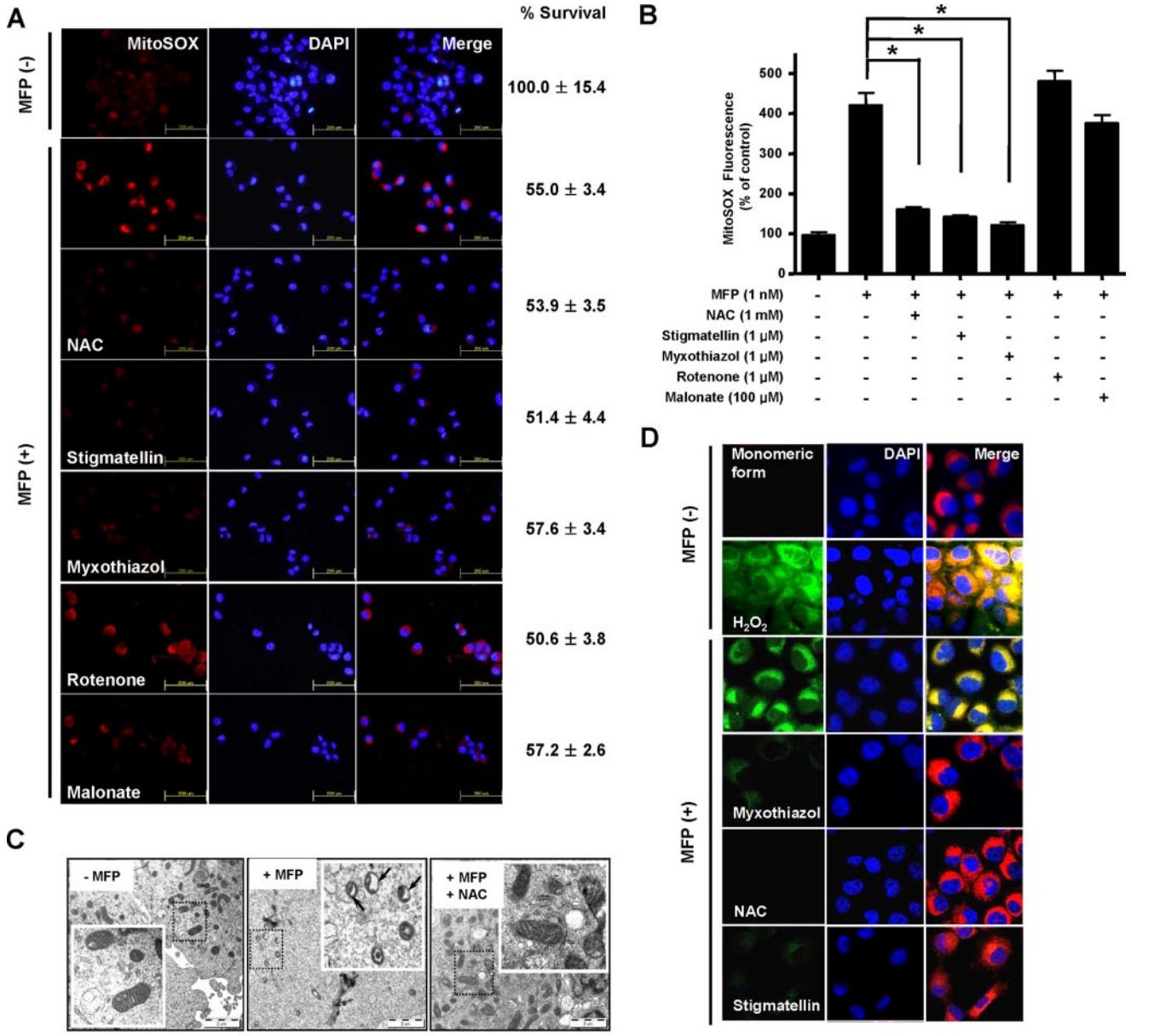

FIGURE 7. **Blockage of Romo1-induced ROS by mitochondrial electron transport chain inhibitors.** *A,* fluorescence microscopy images of Romo1-induced ROS. H1299/pGene-Romo1 treated with MFP (1 nM) for 24 h were cultured in the presence of NAC (1 mM), stigmatellin (1 μM), myxothiazol (1 μM), malonate (100 μM), or rotenone (1 μM). After 1 h, the levels of ROS production were measured by fluorescence microscopy using MitoSOX. *B,* for quantification purposes, exposures were collected for equal times at the same plane of focus. The images were overlaid with a computer, and MitoSOX fluorescence was analyzed with MetaMorph software (Universal Imaging, Westchester, PA). *, $p < 0.001$. *C,* H1299/pGene-Romo1 cells treated with MFP were cultured with or without NAC (0.5 mM) for 24 h. The mitochondrial structure of the cells was examined by transmission electron microscopy. The *white-boxed* region shows a zoomed mitochondrial image of the *dashed box* region. The *arrows* indicate the mitochondria with cristae remodeling. The *scale bar* represents 2 μm. *D,* fluorescence microscopy images of Romo1-induced ΔΨm decrease. The H1299/pGene-Romo1 cells were cells were induced with MFP for 24 h and cultured in the presence of NAC (0.5 mM), myxothiazol (1 μM), or stigmatellin (1 μM) for 30 min. As a positive control, the H1299 cells were treated with hydrogen peroxide (200 μM) for 30 min. Mitochondrial membrane potential levels were determined using JC-1 (5 μM) for 30 min by confocal microscopy. Mitochondria with low ΔΨm exhibited green fluorescence. Merge represents the merged images with *red* plus *green* fluorescence. *DAPI*, 4′,6-diamidino-2-phenylindole.

Therefore, it is possible that Romo1 is located in the mitochondrial membrane and that Romo1 plays an important role in releasing ROS required for cell proliferation into the cytosol. It should be noted that ROS levels are increased from aging and various stresses and that they originate mainly from the mitochondria (3). We postulate that Romo1 expression is induced during aging, and this enhanced Romo1 expression disturbs the mitochondrial respiratory chain, resulting in the excessive generation of ROS. However, further studies will be needed to clarify the exact mechanism by which Romo1 produces ROS and contributes to replicative senescence.

In this study, we showed that increased *Romo1* expression, which is up-regulated in senescing human cells, contributes to replicative senescence by producing ROS persistently and inducing oxidative DNA damage. From the results of this study, we suggest that Romo1 is one of the major molecular contributors toward ROS-associated aging. Further investigations will be required to elucidate the exact mechanism by which Romo1

produces ROS formation. The functional role of Romo1 in aging using an *in vivo* system also remains to be studied. Taken together, our present data demonstrate a new molecule involved in replicative senescence, which should be further studied to understand the aging process.

REFERENCES

1. d'Adda di Fagagna, F., Reaper, P. M., Clay-Farrace, L., Fiegler, H., Carr, P., Von Zglinicki, T., Saretzki, G., Carter, N. P., and Jackson, S. P. (2003) *Nature* **426,** 194–198
2. Shawi, M., and Autexier, C. (2008) *Mech. Ageing Dev.* **129,** 3–10
3. Droge, W. (2002) *Physiol. Rev.* **82,** 47–95
4. Bedard, K., and Krause, K. H. (2007) *Physiol. Rev.* **87,** 245–313
5. Na, A. R., Chung, Y. M., Lee, S. B., Park, S. H., Lee, M. S., and Yoo, Y. D. (2008) *Biochem. Biophys. Res. Commun.* **369,** 672–678
6. Chen, J. H., Hales, C. N., and Ozanne, S. E. (2007) *Nucleic Acids Res.* **35,** 7417–7428
7. Chen, Q., and Ames, B. N. (1994) *Proc. Natl. Acad. Sci. U. S. A.* **91,** 4130–4134
8. Chen, Q., Fischer, A., Reagan, J. D., Yan, L. J., and Ames, B. N. (1995) *Proc. Natl. Acad. Sci. U. S. A.* **92,** 4337–4341
9. Lu, T., and Finkel, T. (2008) *Exp. Cell Res.* **314,** 1918–1922
10. von Zglinicki, T., Saretzki, G., Docke, W., and Lotze, C. (1995) *Exp. Cell Res.* **220,** 186–193
11. Lu, T., Pan, Y., Kao, S. Y., Li, C., Kohane, I., Chan, J., and Yankner, B. A. (2004) *Nature* **429,** 883–891
12. Singh, K. K. (2004) *Ann. N. Y. Acad. Sci.* **1019,** 260–264
13. Hagen, T. M., Yowe, D. L., Bartholomew, J. C., Wehr, C. M., Do, K. L., Park, J. Y., and Ames, B. N. (1997) *Proc. Natl. Acad. Sci. U. S. A.* **94,** 3064–3069
14. Zahn, J. M., Sonu, R., Vogel, H., Crane, E., Mazan-Mamczarz, K., Rabkin, R., Davis, R. W., Becker, K. G., Owen, A. B., and Kim, S. K. (2006) *PLoS Genet.* **2,** e115
15. Linnane, A. W., Marzuki, S., Ozawa, T., and Tanaka, M. (1989) *Lancet* **1,** 642–645
16. Corral-Debrinski, M., Horton, T., Lott, M. T., Shoffner, J. M., Beal, M. F., and Wallace, D. C. (1992) *Nat. Genet.* **2,** 324–329
17. Khaidakov, M., Heflich, R. H., Manjanatha, M. G., Myers, M. B., and Aidoo, A. (2003) *Mutat. Res.* **526,** 1–7
18. Trifunovic, A., Wredenberg, A., Falkenberg, M., Spelbrink, J. N., Rovio, A. T., Bruder, C. E., Bohlooly, Y. M., Gidlof, S., Oldfors, A., Wibom, R., Tornell, J., Jacobs, H. T., and Larsson, N. G. (2004) *Nature* **429,** 417–423
19. Pitkanen, S., and Robinson, B. H. (1996) *J. Clin. Investig.* **98,** 345–351
20. Ishii, N. (2007) *Cornea* **26,** S3–S9
21. Ishii, N., Fujii, M., Hartman, P. S., Tsuda, M., Yasuda, K., Senoo-Matsuda, N., Yanase, S., Ayusawa, D., and Suzuki, K. (1998) *Nature* **394,** 694–697
22. Dufour, E., Boulay, J., Rincheval, V., and Sainsard-Chanet, A. (2000) *Proc. Natl. Acad. Sci. U. S. A.* **97,** 4138–4143
23. Feng, J., Bussiere, F., and Hekimi, S. (2001) *Dev. Cell* **1,** 633–644
24. Migliaccio, E., Giorgio, M., Mele, S., Pelicci, G., Reboldi, P., Pandolfi, P. P., Lanfrancone, L., and Pelicci, P. G. (1999) *Nature* **402,** 309–313
25. Giorgio, M., Migliaccio, E., Orsini, F., Paolucci, D., Moroni, M., Contursi, C., Pelliccia, G., Luzi, L., Minucci, S., Marcaccio, M., Pinton, P., Rizzuto, R., Bernardi, P., Paolucci, F., and Pelicci, P. G. (2005) *Cell* **122,** 221–233
26. Schriner, S. E., Linford, N. J., Martin, G. M., Treuting, P., Ogburn, C. E., Emond, M., Coskun, P. E., Ladiges, W., Wolf, N., Van Remmen, H., Wallace, D. C., and Rabinovitch, P. S. (2005) *Science* **308,** 1909–1911
27. Miwa, S., Riyahi, K., Partridge, L., and Brand, M. D. (2004) *Ann. N. Y. Acad. Sci.* **1019,** 388–391
28. Van Remmen, H., Ikeno, Y., Hamilton, M., Pahlavani, M., Wolf, N., Thorpe, S. R., Alderson, N. L., Baynes, J. W., Epstein, C. J., Huang, T. T., Nelson, J., Strong, R., and Richardson, A. (2003) *Physiol. Genomics* **16,** 29–37
29. Chung, Y. M., Kim, J. S., and Yoo, Y. D. (2006) *Biochem. Biophys. Res. Commun.* **347,** 649–655
30. Hwang, I. T., Chung, Y. M., Kim, J. J., Chung, J. S., Kim, B. S., Kim, H. J., Kim, J. S., and Yoo, Y. D. (2007) *Biochem. Biophys. Res. Commun.* **359,** 304–310
31. Yoo, Y. A., Kim, M. J., Park, J. K., Chung, Y. M., Lee, J. H., Chi, S. G., Kim, J. S., and Yoo, Y. D. (2005) *Mol. Cell. Biol.* **25,** 6603–6616
32. Haendeler, J., Hoffmann, J., Diehl, J. F., Vasa, M., Spyridopoulos, I., Zeiher, A. M., and Dimmeler, S. (2004) *Circ. Res.* **94,** 768–775
33. Atadja, P., Wong, H., Garkavtsev, I., Veillette, C., and Riabowol, K. (1995) *Proc. Natl. Acad. Sci. U. S. A.* **92,** 8348–8352
34. Webley, K., Bond, J. A., Jones, C. J., Blaydes, J. P., Craig, A., Hupp, T., and Wynford-Thomas, D. (2000) *Mol. Cell. Biol.* **20,** 2803–2808
35. Zorov, D. B., Juhaszova, M., and Sollott, S. J. (2006) *Biochim. Biophys. Acta* **1757,** 509–517
36. Stone, J. R., and Yang, S. (2006) *Antioxid. Redox. Signal.* **8,** 243–270
37. Arora-Kuruganti, P., Lucchesi, P. A., and Wurster, R. D. (1999) *J. Neurooncol.* **44,** 213–221
38. Martin, V., Herrera, F., Garcia-Santos, G., Antolin, I., Rodriguez-Blanco, J., and Rodriguez, C. (2007) *Free Radic. Biol. Med.* **42,** 1715–1722
39. Sekharam, M., Trotti, A., Cunnick, J. M., and Wu, J. (1998) *Toxicol. Appl. Pharmacol.* **149,** 210–216
40. Liu, S. L., Lin, X., Shi, D. Y., Cheng, J., Wu, C. Q., and Zhang, Y. D. (2002) *Arch. Biochem. Biophys.* **406,** 173–182
41. Caporossi, D., Ciafre, S. A., Pittaluga, M., Savini, I., and Farace, M. G. (2003) *Free Radic. Biol. Med.* **35,** 1355–1364
42. Sigaud, S., Evelson, P., and Gonzalez-Flecha, B. (2005) *Antioxid. Redox. Signal.* **7,** 6–13
43. Laurent, A., Nicco, C., Chereau, C., Goulvestre, C., Alexandre, J., Alves, A., Levy, E., Goldwasser, F., Panis, Y., Soubrane, O., Weill, B., and Batteux, F. (2005) *Cancer Res.* **65,** 948–956
44. Kregel, K. C., and Zhang, H. J. (2007) *Am. J. Physiol.* **292,** R18–R36
45. Sedelnikova, O. A., Horikawa, I., Zimonjic, D. B., Popescu, N. C., Bonner, W. M., and Barrett, J. C. (2004) *Nat. Cell Biol.* **6,** 168–170
46. Muller, F. L., Liu, Y., and Van Remmen, H. (2004) *J. Biol. Chem.* **279,** 49064–49073